JACS
JOURNAL OF THE AMERICAN CHEMICAL SOCIETY

Article

pubs.acs.org/JACS

How Can We Understand Au_8 Cores and Entangled Ligands of Selenolate- and Thiolate-Protected Gold Nanoclusters $Au_{24}(ER)_{20}$ and $Au_{20}(ER)_{16}$ (E = Se, S; R = Ph, Me)? A Theoretical Study

Nozomi Takagi,[†] Kazuya Ishimura,[‡] Masafuyu Matsui,[†] Ryoichi Fukuda,[†,‡] Toru Matsui,[§] Takahito Nakajima,[§] Masahiro Ehara,[†,‡] and Shigeyoshi Sakaki*[,†,∥,⊥]

[†]Elements Strategy Initiative for Catalysts and Batteries (ESICB), Kyoto University, Kyoto 615-8245, Japan

[‡]Institute for Molecular Science (IMS), Okazaki 444-8585, Japan

[§]RIKEN Advanced Institute for Computational Science (AICS), Kobe 657-0047, Japan

[∥]Fukui Institute for Fundamental Chemistry (FIFC), Kyoto University, Kyoto 606-8103, Japan

[⊥]CREST, Japan Science and Technology Agency (JST), Tokyo 102-0076, Japan

Supporting Information

ABSTRACT: The geometries and electronic structures of selenolate-protected Au nanoclusters, $Au_{24}(SeR)_{20}$ and $Au_{20}(SeR)_{16}$, and their thiolate analogues are theoretically investigated with DFT and SCS-MP2 methods, to elucidate the electronic structure of their unusual Au_8 core and the reason why they have the unusual entangled "staple-like" chain ligands. The Au_8 core is understood to be an $[Au_4]^{2+}$ dimer in which the $[Au_4]^{2+}$ species has a tetrahedral geometry with a closed-shell singlet ground state. The SCS-MP2 method successfully reproduced the distance between two $[Au_4]^{2+}$ moieties, but the DFT with various functionals failed it, suggesting that the dispersion interaction is crucial between these two $[Au_4]^{2+}$ moieties. The SCS-MP2-calculated formation energies of these nanocluster compounds indicate that the thiolate staple-like chain ligands are more stable than the selenolate ones, but the Au_8 core more strongly coordinates with the selenolate staple-like chain ligands than with the thiolate ones. Though $Au_{20}(SeR)_{16}$ has not been reported yet, its formation energy is calculated to be large, suggesting that this compound can be synthesized as a stable species if the concentration of Au(SeR) is well adjusted. The aurophilic interactions between the staple-like chain ligands and between the Au_8 core and the staple-like chain ligand play an important role for the stability of these compounds. Because of the presence of this autophilic interaction, $Au_{24}(SeR)_{20}$ is more stable than $Au_{20}(SeR)_{16}$ and the unusual entangled ligands are involved in these compounds.

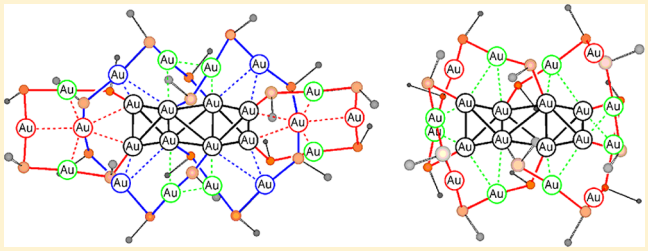

INTRODUCTION

Gold nanoclusters protected by organic ligands[1−4] attract much interests as a building block of novel functional materials such as catalysts, photonics, and molecular electronics,[5,6] because metal nanoclusters exhibit unusual physicochemical properties and chemical reactivity different from bulk metals. Among them, thiolate-protected gold clusters, which are represented with a general $Au_n(SR)_m$ formula, have been widely known.[1] In those compounds, an Au_n core is surrounded by organothiolate (SR) ligands. In many cases, the Au_n core has a highly symmetrical geometry with a closed-shell singlet ground state. Recently, novel thiolate-protected gold clusters $Au_{20}(SR)_{16}$ (R = CH_2CH_2Ph) and $Au_{24}(SR)_{20}$ (R = CH_2CH_2Ph) have been synthesized.[7a,8a] Though their crystal structures have not been reported yet, experimental reports suggest that the Au_8 core is surrounded by four organothiolate ligands such as $Au_3(SR)_4$ and $Au_5(SR)_6$ which have a "staple-like" chain geometry, as shown in Scheme 1a. This type of Au_8 core has never been observed before; very recently, a similar Au_8 core has been experimentally reported in $[Au_8(dppp)_4]^{2+}$, but the number of valence electrons (i.e., the oxidation state of Au) is different.[9] Also, a staple-like chain ligand has been theoretically discussed by one pioneering work[10] and its experimental observation has been limited so far.[11] Moreover, such long staple-like chain ligand as $Au_5(SR)_6$ has not been reported until recent works.[8] What is more interesting is that four $Au_3(SR)_4$ are entangled with each other in $Au_{20}(SR)_{16}$ and two $Au_3(SR)_4$ and two $Au_5(SR)_6$ are entangled in $Au_{24}(SR)_{20}$; see Scheme 1. Several theoretical calculations predicted their possible isomers and suggested that the relation between the geometry and the absorption spectrum is useful to discuss the geometries of these thiolate-protected Au nanoclusters.[7b,8b]

Very recently, the first X-ray analysis of a similar selenolate-protected Au nanocluster compound $Au_{24}(SeR)_{20}$ (R = Ph) **1-SePh** was successfully made.[12] As suggested for the thiolate analogue $Au_{24}(SR)_{20}$,[8b] **1-SePh** consists of an Au_8 core with two

Received: April 27, 2015
Published: June 15, 2015

DOI: 10.1021/jacs.5b04337
J. Am. Chem. Soc. 2015, 137, 8593−8602

Scheme 1. Schematic Representations of (a) $Au_{24}(ER)_{20}$ 1-ER and $Au_{20}(ER)_{16}$ 2-ER (E = S or Se), (b) $Au_3(ER)_4$, and (c) $Au_5(ER)_6$ Staple-like Chain Ligands

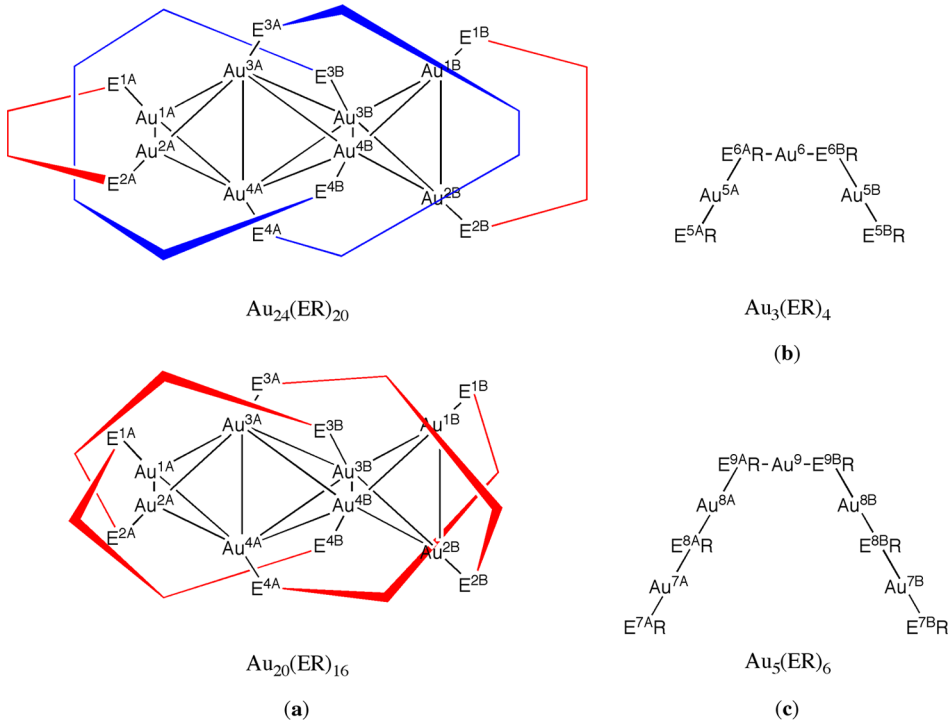

$Au_3(SeR)_4$ and two $Au_5(SeR)_6$ staple-like chain ligands, as shown in Scheme 1. This work is of considerable interest in the chemistry of nanocluster, because the experimental evidence of the Au_8 core and the entangled geometries of the staple-like chain ligands were clearly shown. However, the reason for such geometries is unclear; important questions to be answered are found; (1) why the Au_8 core is stable in this compound, (2) what electronic structure the Au_8 core has, (3) how much these clusters are stabilized by the staple-like chain ligands, (4) why the staple-like chain ligands are entangled, and (5) why two similar thiolate-protected nanoclusters $Au_{20}(SR)_{16}$ and $Au_{24}(SR)_{20}$ have been reported but only one $Au_{24}(SeR)_{20}$ has been reported in the selenolate case; in other words, how and why the thiolate and selenolate Au clusters are different.

Though several theoretical studies have been carried out for these thiolate-protected Au nanoclusters,[7b,8b] no theoretical answer has been presented on the above-mentioned questions. In this work, we theoretically investigated the geometries and the electronic structures of $Au_{24}(SeR)_{20}$ **1-SeR**, $Au_{20}(SeR)_{16}$ **2-SeR** (R = Ph and Me), and their thiolate analogues to provide theoretical answers to those questions. We believe that the theoretical answers to these questions provide correct understanding of the similar Au cluster compounds and therefore contributes to further development in the chemistry of Au nanoclusters.

COMPUTATIONAL DETAILS AND MODELS

In this work, several Au−Au distances were optimized with the spin-component-scaled MP2 (SCS-MP2) method[13] and the other moieties were optimized by DFT method with the B3PW91 functional,[14,15] after testing various functionals such as PBE,[16] M06L,[17] B3LYP,[14,18] TPSSh,[19] M06,[20] B3LYP-D,[14,18,21] and B3LYP-D3.[14,18,22] For Au, the LANL2DZ basis set was employed,[23a] where the core electrons were replaced with the effective core potentials (ECPs).[23a] For S and Se, the LANL2DZ basis sets were employed with the ECPs,[23b] where one d polarization function was added.[24] The 6-31G(d) basis sets were employed for C and H.[25] This basis set system is named BS-1. A better basis set system, named BS-2, was employed for the evaluation of energy and the analysis of electronic structure. In BS-2, a (311111/22111/411) basis set was employed for Au with the ECPs of the Stuttgart-Dresden-Bonn (SDB) group,[26] where f polarization function was not added; see ref 27 for the effects of f polarization function. The (31/311/1) basis sets were employed for S and Se with the SDB ECPs.[26,28] The 6-311G(d) basis sets were employed for C and H. The energy was evaluated with the SCS-MP2 method. DFT calculations were carried out with the *Gaussian09* program,[29] and MP2 calculations were carried out with the *NTChem*[30] and *SMASH*[31] programs.

$Au_{24}(SePh)_{20}$, $Au_{24}(SCH_2CH_2Ph)_{20}$, and $Au_{20}(SCH_2CH_2Ph)_{16}$ were experimentally investigated.[7a,8a,12] In the present calculations, the SePh group was employed without modification, while the SCH_3 (SMe) group was used as a model of the SCH_2CH_2Ph group to save CPU time.

RESULTS AND DISCUSSION

1. Geometry of $Au_{24}(SePh)_{20}$ and Importance of Aurophilic Interaction. The geometry of $Au_{24}(SePh)_{20}$ **1-SePh** was fully optimized without any constraint by various DFT functionals. However, no DFT functional reproduces well the geometry of **1-SePh**, as summarized below: (i) Hybrid fuctionals fail to describe the Au^{3A}−Au^{3B}, Au^{3A}−Au^{4B}, Au^{4A}−Au^{3B}, and Au^{4A}−Au^{4B} distances in the Au_8 core; see Scheme 1 for Au^{3A}, etc. (ii) Pure functionals fail to reproduce the Au−Se distances. And, (iii) dispersion-corrected functionals fail to reproduce the structure of the Au_8 core; see Table S1, Figure S1, and discussion there in the Supporting Information.

These results suggest that post-Hartree−Fock methods such as MP2 to MP4 and CCSD(T) must be applied to the geometry optimization of this Au nanocluster compound and analogues. However, such calculation is nearly impossible due to the large size of **1-SePh**. One of the reasonable ways is to use a combination of DFT and post-Hartree−Fock methods, because the DFT with the B3PW91 functional reproduces the geo-

DOI: 10.1021/jacs.5b04337
J. Am. Chem. Soc. 2015, 137, 8593−8602

metrical parameters except for the Au^{3A}–Au^{3B}, Au^{3A}–Au^{4B}, Au^{4A}–Au^{3B}, and Au^{4A}–Au^{4B} distances and the MP2 and SCS-MP2 are expected to reproduce well these distances because the MP2 and SCS-MP2 are useful to investigate aurophilic interaction.[32] We employed here the MP2 and SCS-MP2 for optimizing the Au^{3A}–Au^{3B}, Au^{3A}–Au^{4B}, Au^{4A}–Au^{3B}, and Au^{4A}–Au^{4B} distances and the DFT with the B3PW91 for optimizing the other moiety. This procedure is named hereafter MP2:B3PW91 and SCS-MP2:B3PW91.

The potential energy curves against the X^1–X^2 distance were evaluated with these combined methods, as shown in Figure 1,[33]

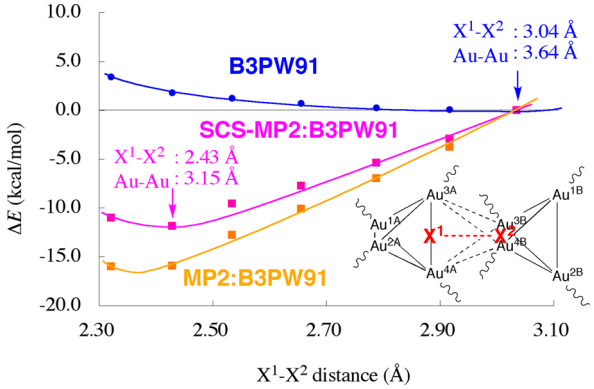

Figure 1. Potential energy curves against the X^1–X^2 distance (The X^1 and X^2 are the midpoints of Au^{3A}–Au^{4A} and Au^{3B}–Au^{4B} bonds, respectively.) of **1-SePh** at the B3PW91/BS-1 (blue), the MP2:B3PW91 (orange), and the SCS-MP2:B3PW91 (magenta) levels.

where the X^1 and X^2 are the midpoints of the Au^{3A}–Au^{4A} and Au^{3B}–Au^{4B} bonds, respectively. The energy minimum was located around $R(X^1–X^2)$ = 3.04 Å ($R(Au–Au)_{ave}$ = 3.64 Å) by the B3PW91 optimization, where the $R(Au–Au)_{ave}$ is the average of the Au^{3A}–Au^{3B}, Au^{3A}–Au^{4B}, Au^{4A}–Au^{3B}, and Au^{4A}–Au^{4B} distances. These distances are much longer than the experimental values; $R(X^1–X^2)$ = 2.58 Å and $R(Au–Au)_{ave}$ = 3.22 Å. On the other hand, the energy minimum is found at $R(X^1–X^2)$ = 2.38 Å ($R(Au–Au)_{ave}$ = 3.11 Å) in the MP2:B3PW91 optimization and at $R(X^1–X^2)$ = 2.43 Å ($R(Au–Au)_{ave}$ = 3.15 Å) in the SCS-MP2:B3PW91 optimization. This SCS-MP2:B3PW91-optimized distance is closer to the experimental value than the MP2:B3PW91-optimized one. Thus-optimized SCS-MP2:B3PW91 geometry agrees with the experimental one, as shown in Figure 2.

On the basis of these results, it is concluded that the aurophilic interaction plays crucial roles in determining the geometry of the Au_8 core. This means that the geometry of Au nanocluster compound must be carefully optimized with the appropriate method that can describe well the aurophilic interaction.

2. Electronic Structure and Geometry of the Au_8 Core in $Au_{24}(SePh)_{20}$. One of the characteristic features of **1-SePh** is the geometry of the Au_8 core surrounded by such staple-like chain ligands as $Au_3(SePh)_4$ and $Au_5(SePh)_6$, as mentioned above; see also Scheme 1a. However, no detailed discussion has been presented about the unusual structure of the Au_8 core. According to the general knowledge of coordination chemistry, the staple-like chain ligand $Au_3(SePh)_4$ can be understood to consist of three Au(I) cations and four $SePh^-$ anions (Scheme 1b). The $Au_5(SePh)_6$ is similarly understood to consist of five Au(I) cations and six $SePh^-$ anions (Scheme 1c). This means that these ligands have −1 charge. Because **1-SePh** is neutral, **1-SePh** is understood to consist of the Au_8 core with +4 charges, two $Au_3(SePh)_4$, and two $Au_5(SePh)_6$ anion ligands. Considering the Au^{3A}–Au^{3B}, Au^{3A}–Au^{4B}, Au^{4A}–Au^{3B}, and Au^{4A}–Au^{4B} distances are much longer than the other Au^{1A}–Au^{3A}, Au^{1A}–Au^{2A}, Au^{1A}–Au^{4A}, and Au^{3A}–Au^{4A} distances by about 0.5 Å, as shown in Table S1 in the Supporting Information, it is likely that the $[Au_8]^{4+}$ core consists of two $[Au_4]^{2+}$ species; in other words, the $[Au_8]^{4+}$ core is a dimer of $[Au_4]^{2+}$. This understanding is consistent with the computational result that the usual hybrid functionals somewhat overestimate the Au^{3A}–Au^{3B}, Au^{3A}–Au^{4B}, Au^{4A}–Au^{3B}, and Au^{4A}–Au^{4B} distances, which correspond to the distance between two $[Au_4]^{2+}$ moieties.

The isolated $[Au_4]^{2+}$ is calculated to have a tetrahedral structure (T_d) with a closed-shell singlet ground state, as reported previously in theoretical[34a] and experimental works.[34b] This is much more stable than a square planar one (D_{4h}) by 26.6 kcal/mol, where the SCS-MP2 method was employed. In the T_d structure, the B3PW91-optimized Au–Au distance of 2.78 Å is close to the experimental value (2.74 Å) of the $[Au_4]^{2+}$ moiety in **1-SePh**. The triplet state of $[Au_4]^{2+}$ has a D_2-like deformed structure with Au–Au distances of 2.57 and 2.80 Å. This is 71.8 kcal/mol above the T_d structure with a singlet ground state. The D_{4h} planar structure of $[Au_4]^{2+}$ with a closed-shell singlet state is not located as an energy minimum because it has two imaginary frequencies. The linear structure of $[Au_4]^{2+}$ is not located as a local minimum with four imaginary frequencies, too. This is 63.1 kcal/mol above. All these results indicate that the $[Au_4]^{2+}$ moiety has the T_d structure with a closed-shell singlet ground state.

The reason why the closed-shell singlet is the ground state is easily understood in terms of orbital picture shown in Scheme 2. Because the Au atom has a $5d^{10}6s^1$ electron configuration, the 6s orbital mainly participates in the bonding orbital. In the D_{4h} structure, the ${\varphi_1}^{D_{4h}}$ is the most stable, the degenerate ${\varphi_2}^{D_{4h}}$ and ${\varphi_3}^{D_{4h}}$ are next, and the ${\varphi_4}^{D_{4h}}$ is the least stable. The bonding combination of the d_{z^2} orbitals mixes into the ${\varphi_1}^{D_{4h}}$ in an antibonding way with the 6s orbitals, because they belong to the same symmetry and the d_{z^2} exists at a lower energy than the 6s orbital in Au. Among these four MOs, only the most stable ${\varphi_1}^{D_{4h}}$ is doubly occupied, as shown in Scheme 2, since two 6s electrons are involved in the $[Au_4]^{2+}$ species. In the T_d structure, the most stable MO is nondegenerated ${\varphi_1}^{T_d}$ and three degenerate ${\varphi_2}^{T_d}$ to ${\varphi_4}^{T_d}$ are above ${\varphi_1}^{T_d}$. Hence, only the ${\varphi_1}^{T_d}$ is doubly occupied, too. These results indicate that the closed-shell singlet is the ground state in the $[Au_4]^{2+}$ species with both of the D_{4h} and T_d structures. The next question to be investigated is the reason why the $[Au_4]^{2+}$ species has the T_d structure. As shown in Scheme 2, the φ_1 is more stable in the T_d structure than in the D_{4h} one; see Figure S2 in the Supporting Information for the detailed orbital energy levels. This result is easily interpreted in terms of the bonding interaction, as follows: In the ${\varphi_1}^{D_{4h}}$, four 6s–6s bonding overlaps are involved. In the ${\varphi_1}^{T_d}$, six 6s–6s bonding overlaps are involved. Hence, the ${\varphi_1}^{T_d}$ is more stable than the ${\varphi_1}^{D_{4h}}$. On the basis of these results, it is concluded that the doubly occupied ${\varphi_1}^{T_d}$ is more stable in energy than the ${\varphi_1}^{D_{4h}}$, which is the reason why the T_d structure is more stable than the D_{4h} one.

In the Au_8 core, the edge of one $[Au_4]^{2+}$ species is not parallel but perpendicular to that of another $[Au_4]^{2+}$ species; see Scheme 1. It is interesting to elucidate whether its geometry arises from the coordination of the staple-like chain ligand or the intrinsic feature of the $[Au_8]^{4+}$ core. We calculated the parallel conformation (**Conf-I**) and the perpendicular one (**Conf-II**) of the $[Au_8]^{4+}$ core at the SCS-MP2 level. As shown in Figure 3, the $[Au_8]^{4+}$ core becomes more stable as going from **Conf-I** to

DOI: 10.1021/jacs.5b04337
J. Am. Chem. Soc. 2015, 137, 8593–8602

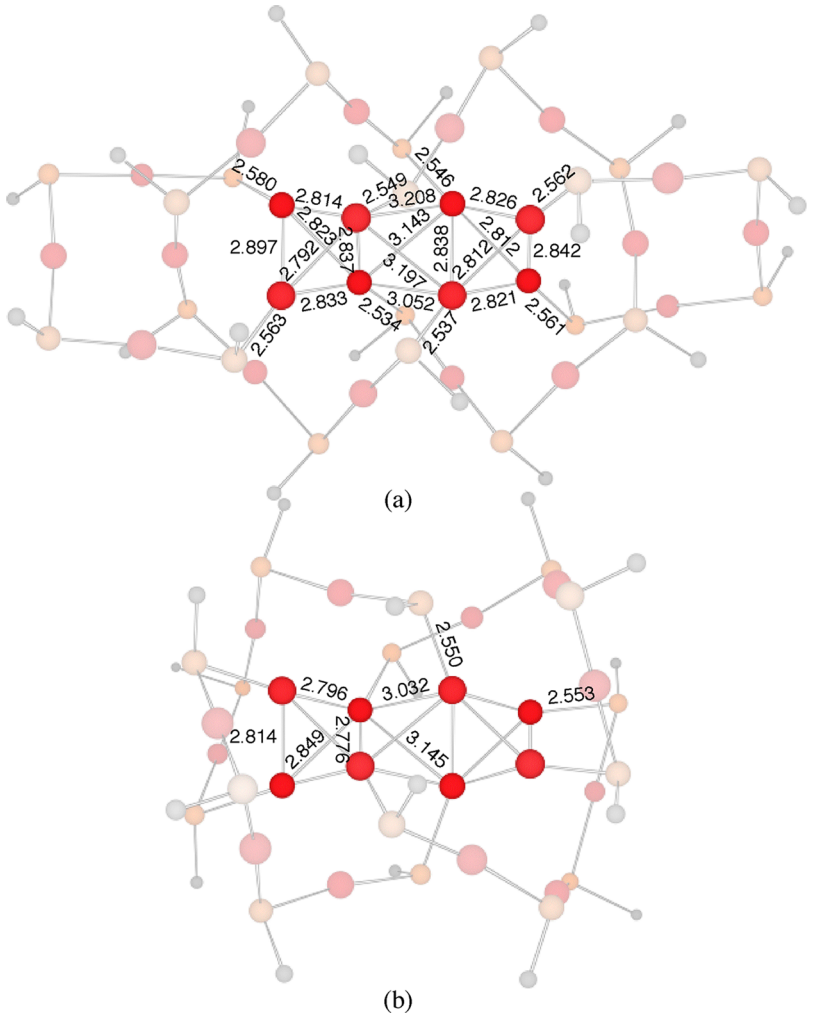

Figure 2. Optimized structures (distances are in angstrom; Ph groups are omitted for clarity) of the selenolate-protected Au nanocluster (a) $Au_{24}(SePh)_{20}$ **1-SePh** and (b) $Au_{20}(SePh)_{16}$ **2-SePh** at the SCS-MP2:B3PW91 level. (The Au^{3A}–Au^{3B}, Au^{3A}–Au^{4B}, Au^{4A}–Au^{3B}, and Au^{4A}–Au^{4B} distances were optimized by the SCS-MP2 and the other moiety was optimized at the B3PW91/BS-1 level.)

Scheme 2. Molecular Orbitals Consisting of Four 6s Orbitals of Au in $[Au_4]^{2+}$ Taking the Square Planar (D_{4h}) or the Tetrahedral (T_d) Structure[a]

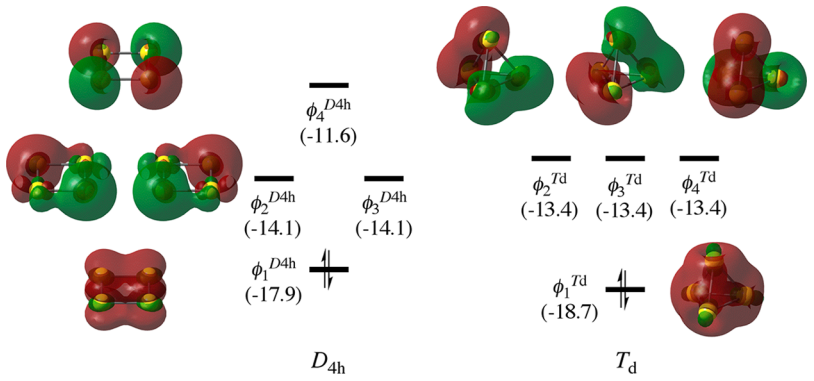

[a]The B3PW91/BS-2//B3PW91/BS-1 method was employed.

Conf-II. This result clearly shows that the larger stability of **Conf-II** arises from the intrinsic character of the $[Au_8]^{4+}$ core. To clarify the reason, the relative energy and important MOs are plotted against the dihedral angle θ between two edges. Apparently, three antibonding MOs are found in **Conf-I**. As going from **Conf-I** to **Conf-II**, one of them (φ_1^{Au8}) becomes more stable in energy because it is purely nonbonding in **Conf-II**; see ref 35 for the reason why it is the most stable around $\theta = 55°$ and then becomes moderately less stable in **Conf-II**. Also, the steric repulsion is more favorable in **Conf-II** than in **Conf-I**. Hence, **Conf-II** is more stable than **Conf-I**; in other words, the $[Au_8]^{4+}$ core takes a perpendicular structure.

DOI: 10.1021/jacs.5b04337
J. Am. Chem. Soc. 2015, 137, 8593−8602

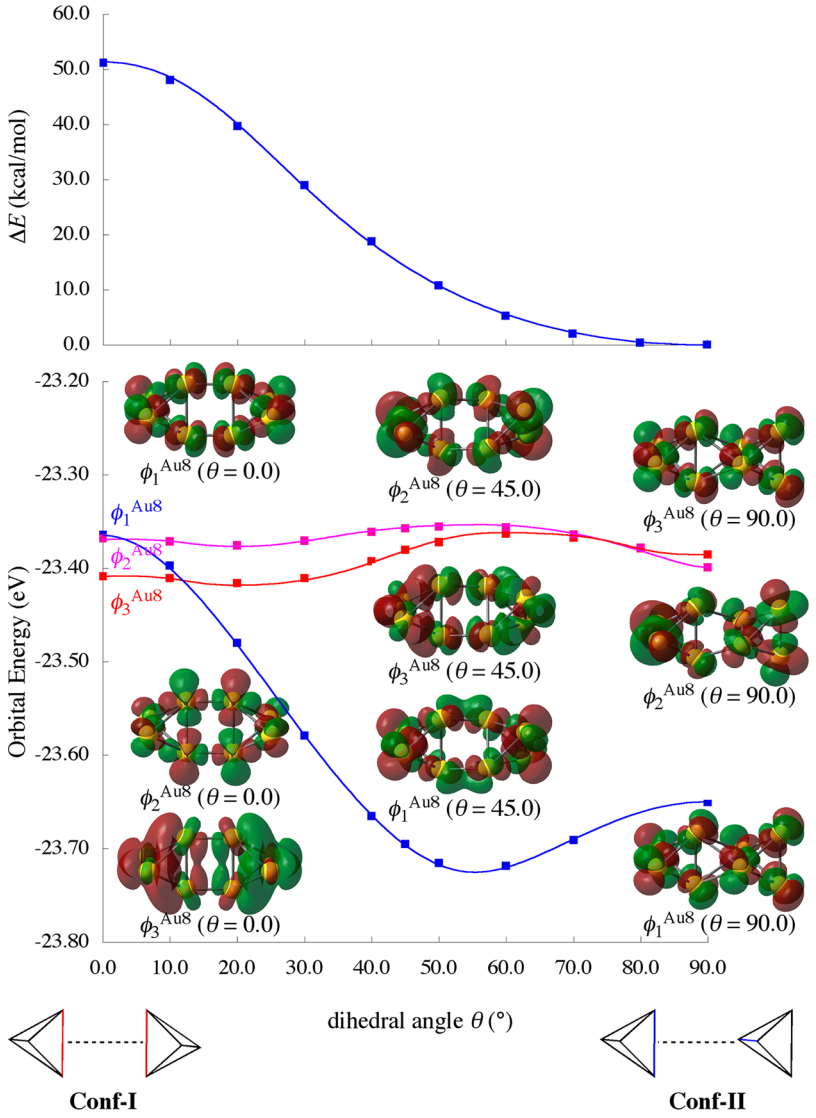

Figure 3. Changes in stability of $[Au_8]^{4+}$ (in kcal/mol) [The SCS-MP2/BS-2//B3PW91/BS-1 levels, where the X^1–X^2 was taken to be the same as that (2.43 Å) of **1-SePh**] and orbital energy (eV) [the B3PW91/BS-2//B3PW91/BS-1 levels] against the dihedral angle (θ) between two edges of two $[Au_4]^{2+}$ moieties.

Table 1. Formation Energies (in kcal/mol)[a] of $[Au_3(ER)_4]^-$ and $[Au_5(ER)_6]^-$ Ligands, $Au_{24}(ER)_{20}$ (1-ER) and $Au_{20}(ER)_{16}$ (2-ER) from the Sum of Tetrahedral-$[Au_4]^{2+}$, $[ER]^-$, and Cyclic-$[Au(ER)]_4$ (E = S and Se; R = Ph and Me)

		formation of $4[Au_3(ER)_4]^-$	formation of $2[Au_5(ER)_6]^-$	formation of $4[Au_3(ER)_4]^-+2[Au_5(ER)_6]^-$	formation of **1-ER**	formation of **2-ER**
	$2[Au_4]^{2+}$	$2[Au_4]^{2+}$	$2[Au_4]^{2+}$	$2[Au_4]^{2+}$	$Au_{24}(ER)_{20}$;**1-ER**	$Au_{20}(ER)_{16}$; **2-ER**
	$6[ER]^-$	$4[Au_3(ER)_4]^-$	$4[ER]^- + 6/2[Au(ER)]_4$	$4[Au_3(ER)_4]^-$	$2[Au_3(ER)_4]^-$	$2[Au_5(ER)_6]^-$
	$11/2[Au(ER)]_4$	$2[ER]^- + 5/2[Au(ER)]_4$	$2[Au_5(ER)_6]^-$	$2[Au_5(ER)_6]^-$		
			R = Ph			
E = Se	0.0	−147.3 (−36.8)[b]	−85.1 (−42.6)[b]	−232.5	−1516.8 [−1284.3][c]	−1376.1 [−1143.6][c]
E = S	0.0	−152.4 (−38.1)[b]	−86.2 (−43.1)[b]	−238.6	−1495.9 [−1257.3][c]	−1369.6 [−1131.0][c]
			R = Me			
E = Se	0.0	−166.2 (−41.5)[b]	−93.2 (−46.6)[b]	−259.3	−1447.4 [−1188.1][c]	−1372.8 [−1113.5][c]
E = S	0.0	−175.7 (−43.9)[b]	−99.6 (−49.8)[b]	−275.3	−1440.9 [−1165.6][c]	−1377.6 [−1102.3][c]

[a]The SCS-MP2/BS-2//B3PW91/BS-1 method was employed, while **1-ER** and **2-ER** were optimized with the SCS-MP2:B3PW91 method. [b]Formation energy per one ligand is shown in the parentheses. [c]The coordination energy between the $[Au_8]^{4+}$ core and staple-like chain ligand is shown in the square bracket.

3. Formation Energies of $Au_{24}(SePh)_{20}$ and $Au_{20}(SePh)_{16}$. If the $[Au_4]$ moiety has +2 charge, the electrostatic interaction between two $[Au_4]$ moieties is very repulsive. However, the real charge of the $[Au_4]$ moiety is not +2 but much smaller in these nanocluster compounds, because charge-transfer significantly occurs from the staple-like chain

DOI: 10.1021/jacs.5b04337
J. Am. Chem. Soc. 2015, 137, 8593−8602

Scheme 3. Schematic Representations of Coordination of the $[Au_4]^{2+}$ Species with the Staple-like Chain Ligands (a) Two $[Au_3(SePh)_4]^-$ and (b) Two $[Au_5(SePh)_6]^-$

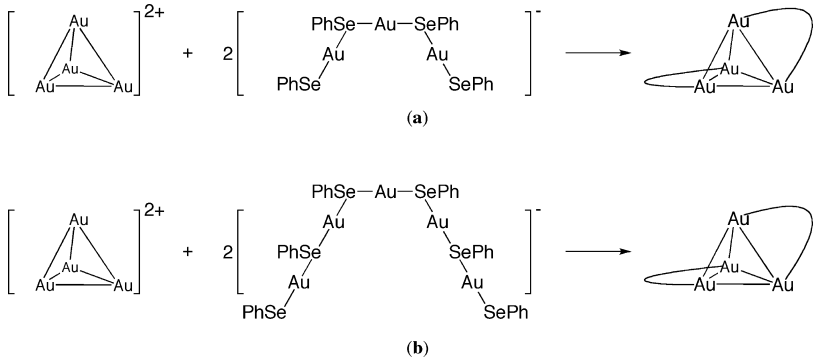

ligands to the $[Au_4]^{2+}$ moiety; see ref 36. Hence, we investigated how much two $[Au_4]^{2+}$ moieties are stabilized by the coordination of the staple-like chain ligands. The formation energies of the staple-like chain ligands, $[Au_3(SePh)_4]^-$ and $[Au_5(SePh)_6]^-$, and Au nanocluster compounds, $Au_{24}(SePh)_{20}$ **1-SePh** and $Au_{20}(SePh)_{16}$ **2-SePh**, were evaluated, as summarized in Table 1, where the sum of two $[Au_4]^{2+}$, six $[SePh]^-$, and 5.5 molecules of cyclic-$[Au(SePh)]_4$[37] was taken as the standard.[38] Though **2-SePh** has not been experimentally reported, this compound is investigated here for a comparison with **1-SePh**. The formation energies of the $[Au_3(SePh)_4]^-$ and $[Au_5(SePh)_6]^-$ ligands are calculated to be 36.8 and 42.6 kcal/mol, respectively, at the SCS-MP2 level. The formation energy of $[Au_5(SePh)_6]^-$ is larger than that of $[Au_3(SePh)_4]^-$, because the former has 10 Au−Se bonds but the latter has six Au−Se bonds.

The formation energy of **1-SePh** + $2[Au_3(SePh)_4]^-$ is calculated to be 1516.8 kcal/mol. That of **2-SePh** + $2[Au_5(SePh)_6]^-$ (1376.1 kcal/mol) is significantly smaller than that of **1-SePh** + $2[Au_3(SePh)_4]^-$ by 140.7 kcal/mol. Because the formation energy of $[Au_5(SePh)_6]^-$ is larger than that of the $[Au_3(SePh)_4]^-$, it is concluded that the formation energy of **1-SePh** is larger than that of **2-SePh**. The coordination energy per one Se atom in the staple-like chain ligand with the Au_8 core is evaluated to be 160.5 kcal/mol in **1-SePh**, which is considerably larger than that (143.0 kcal/mol) in **2-SePh** against our expectation that the coordination energy per one Se atom is not so much different between these two compounds. The reason the coordination energy is larger in **1-SePh** than in **2-SePh** is of considerable interest. The HOMO energy of $[Au_5(SePh)_6]^-$ (−3.15 eV) is somewhat lower than that of $[Au_3(SePh)_4]^-$ (−2.92 eV), while the shape of the HOMO is essentially the same between them; see Figure S3 in the Supporting Information. Thus, the HOMO energy is not responsible for the larger coordination energy in **1-SePh** than in **2-SePh**. It is noted that the ligands in **1-SePh** are more entangled with each other than in **2-SePh**. This fact suggests that one of the possible reasons of the larger coordination energy of **1-SePh** is an attractive interaction between the ligands. To investigate if the ligand−ligand attractive interaction contributes to the coordination energy, we calculated the coordination energy between one $[Au_4]^{2+}$ core and two staple-like chain ligands, where the ligand−ligand interaction is absent, as shown in Scheme 3. The coordination energy between one $[Au_4]^{2+}$ core and two $[Au_3(SePh)_4]^-$ ligands is 121.8 kcal/mol per one Se atom, which is moderately smaller than that between one $[Au_4]^{2+}$ core and two $[Au_5(SePh)_6]^-$ ligands (124.5 kcal/mol per one Se atom). The HOMO energy of the $[Au_5(SePh)_6]^-$ ligand is lower than that of the $[Au_3(SePh)_4]^-$ ligand, as shown in Table 2. Therefore, this HOMO is not responsible for the larger coordination energy per one Se atom in **1-SePh** than in **2-SePh**. Also, it is noted that the coordination energy of the $[Au_4]^{2+}$ core per one Se atom is much smaller than in **1-SePh** and **2-SePh**. Thus, it is concluded that the ligand−ligand interaction plays a crucial role in providing the larger coordination energy of **1-SePh** than that of **2-SePh**, which will be discussed in detail in the next section.

Table 2. Valence Orbital Energies (in eV) of ·ER (SOMO), $[Au_3(ER)_4]^-$ (HOMO), and $[Au_5(ER)_6]^-$ (HOMO) at the HF/BS-2//B3PW91/BS-1 Method[a]

	·ER	$[Au_3(ER)_4]^-$	$[Au_5(ER)_6]^-$
	SOMO energy	HOMO energy	HOMO energy
		E = S	
R = Me	−10.08	−5.27	−5.59
R = Ph	−8.52	−5.03	−5.23
		E = Se	
R = Me	−9.39	−4.93	−5.22
R = Ph	−8.38	−4.90	−5.11

[a]The geometries of these species were optimized by the DFT with the B3PW91 functional.

4. Interaction between Staple-like Chain Ligands in $Au_{24}(SePh)_{20}$ and $Au_{20}(SePh)_{16}$. To evaluate the interaction energy between Au atoms in the entangled staple-like chain ligands, the potential energy curve against the Au−Au distance between two cyclic-$[Au(SeMe)]_4$ molecules was calculated at the SCS-MP2 level, as shown in Figure 4.[39] It is likely that the electronic structure of Au atom is not very different between cyclic-$[Au(SeMe)]_4$ and the staple-like chain ligands in **1-SePh** and **2-SePh**. In Figure 4, an attractive interaction between two Au atoms is found to be about 10−15 kcal/mol around the Au−Au distance of 3.5 Å, suggesting that the Au−Au interaction is formed around the Au−Au distance of 3.5 Å; see Supporting Information Figure S4 for the comparison between MP2- and DFT-calculated potential energy curves.

In **1-SePh** and **2-SePh**, the Au atoms in the staple-like chain ligands are classified into three types, as shown in Figure 5a; central (red), middle (blue), and terminal (green) in $Au_5(SePh)_6$, central (red) and terminal (green) in $Au_3(SePh)_4$. Considering that the Au−Au interaction is formed around an Au−Au distance of 3.5 Å, the Au−Au distances between two staple-like chain ligands and between the Au_8 core and the staple-like chain ligand within 3.5 Å are represented by a dashed line; see Figure 5b. The central Au atom (red) forms 10 interactions

DOI: 10.1021/jacs.5b04337
J. Am. Chem. Soc. 2015, 137, 8593−8602

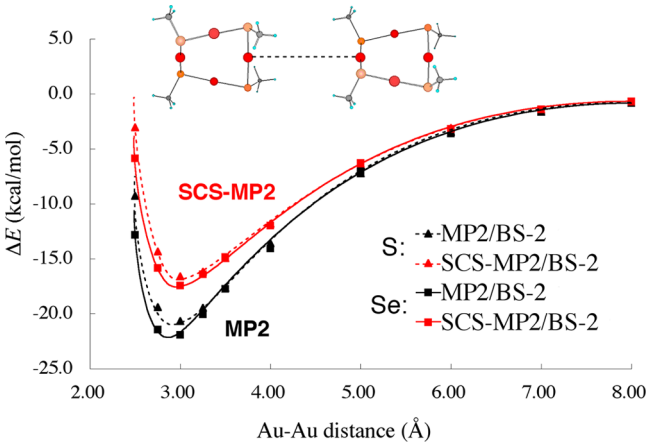

Figure 4. Potential energy curves [the MP2/BS-2//B3PW91/BS-1 (black) and the SCS-MP2/BS-2//B3PW91/BS-1 (red) methods were employed] against the Au−Au distance between two cyclic-$[Au(EMe)]_4$ (E = S and Se) molecules.

with neighboring Au atoms in **1-SePh**. The middle (blue) and the terminal (green) Au atoms form eight and six interactions with neighboring Au atoms, respectively. Thereby, totally, 24 Au−Au interactions are formed in **1-SePh**. In **2-SePh**, on the other hand, the central Au atom (red) does not form any interaction but the terminal Au atom (green) forms 12 interactions with neighboring Au atoms, which is just one-half of **1-SePh**. It is likely that these Au−Au interactions contribute more to the stabilization of **1-SePh** than to that of **2-SePh**. The difference in the sum of the Au−Au interaction energies between **1-SePh** and **2-SePh** is about 12 × (10−15 kcal/mol) = 120−180 kcal/mol, which is comparable to the difference in the coordination energy between **1-SePh** and **2-SePh** (140.7 kcal/mol). It is concluded that the larger stabilization energy of **1-SePh** than that of **2-SePh** arises from the attractive interactions between staple-like chain ligands and between the Au_8 core and the staple-like chain ligand. This attractive Au−Au interaction stabilizes the entangled geometry of these ligands because the Au−Au distance becomes short in such entangled geometry.

5. Comparisons between Thiolate- and Selenolate-Protected Au Nanoclusters. Though the selenolate-protected Au nanocluster **2-SePh** has not been isolated yet, the thiolate analogue $Au_{20}(SR)_{16}$ **2-SR** (R = CH_2CH_2Ph) as well as $Au_{24}(SR)_{20}$ **1-SR** has been experimentally reported with the UV−vis spectra.[7a,8a] Theoretical calculations indicated that the Au_8 core is surrounded by such staple-like chain ligands as $[Au_3(SR)_4]^-$ and $[Au_5(SR)_6]^-$ in these compounds.[7b,8b] The formation energies of these thiolate analogues from two $[Au_4]^{2+}$, six $[SMe]^-$, and 5.5 molecules of cyclic-$[Au(SMe)]_4$ were evaluated in a similar manner to that of **1-SePh**, as summarized in Table 1, where methyl (Me) group was employed as a model of CH_2CH_2Ph; these thiolate analogues are named **1-SMe** and **2-SMe**, respectively. Their optimized geometries are shown in Figure S5 in the Supporting Information.

The formation energy of the staple-like $[Au_3(SMe)_4]^-$ and $[Au_5(SMe)_6]^-$ ligands are 43.9 and 49.8 kcal/mol, respectively. The sum of the formation energies of four $[Au_3(SMe)_4]^-$ and two $[Au_5(SMe)_6]^-$ is 275.3 kcal/mol, which is somewhat larger than those of the selenolate analogues. The same trend is observed in R = Ph. This is because the Au−SMe and Au−SPh bond energies (47.1 and 52.0 kcal/mol, respectively) are larger than the Au−SeMe and Au−SePh ones (44.9 and 49.5 kcal/mol, respectively).

The stronger Au−SR bond than the Au−SeR one can be explained by the SOMO energy levels of ·SR and ·SeR. An A−B covalent bond energy E_{BE} is approximately represented by eq 1 based on the simple Hückel MO method;

$$E_{BE} = \{(\varepsilon_A - \varepsilon_B)^2 + 4\beta^2\}^{1/2} \quad (1)$$

where ε_A and ε_B are orbital energies of valence orbitals χ_A and χ_B, respectively, and β is a resonance integral.[40] This eq says that the covalent bond energy increases as the $|\varepsilon_A - \varepsilon_B|$ value becomes

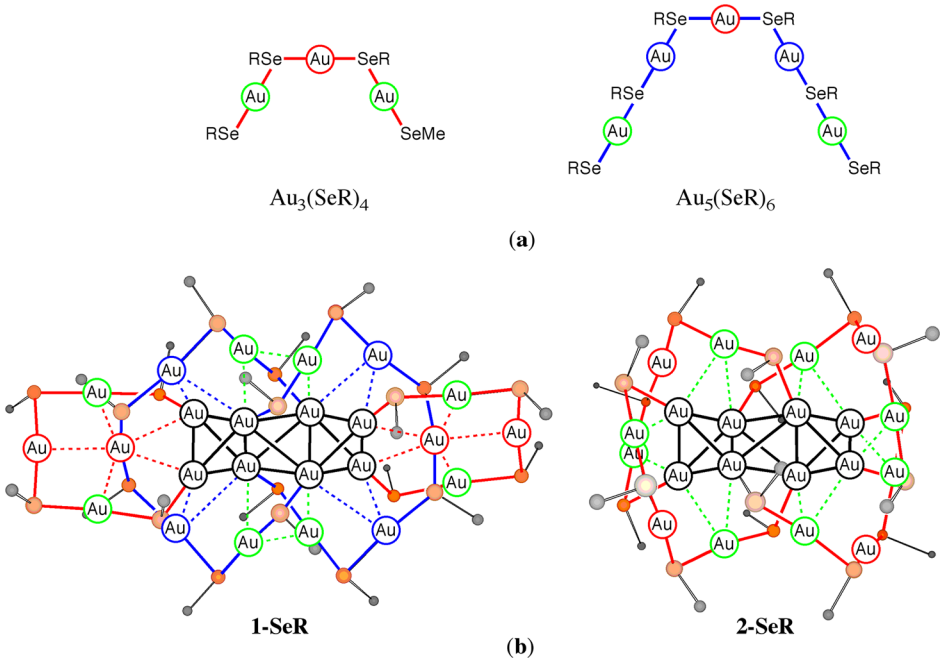

Figure 5. (a) Schematic representations of central Au (red), middle Au (blue), and terminal Au (green) in staple-like chain ligands $Au_3(SeR)_4$ and $Au_5(SeR)_6$, and (b) **1-SeR** and **2-SeR**. The Au−Au distance shorter than 3.5 Å is represented by a dashed line.

DOI: 10.1021/jacs.5b04337
J. Am. Chem. Soc. 2015, 137, 8593−8602

large. The valence 6s orbital of the Au exists at a higher energy (−7.94 eV) than those of ·SR and ·SeR and the valence orbital of ·SR exists at a lower energy than that of ·SeR, as shown in Table 2. Because the $|\varepsilon_A - \varepsilon_B|$ is larger in the thiolate case than in the selenolate case, the Au-SR bond is stronger than the Au−SeR bond. It is concluded that the valence orbital of ·SR at a lower energy than that of ·SeR leads to the larger formation energy of the thiolate staple-like chain ligand than that of the selenolate one.

Despite of the larger formation energy of the thiolate staple-like chain ligand than the selenolate one, the formation energies of **1-SMe** + $2[Au_3(SMe)_4]^-$ (1440.9 kcal/mol) and **1-SPh** + $2[Au_3(SPh)_4]^-$ (1495.9 kcal/mol) are smaller than those of **1-SeMe** + $2[Au_3(SeMe)_4]^-$ (1447.4 kcal/mol) and **1-SePh** + $2[Au_3(SePh)_4]^-$ (1516.8 kcal/mol), respectively, as shown in Table 1. This is because the coordination energy of the Au_8 core with selenolate staple-like chain ligands is significantly larger than that with the thiolate analogues; see that the difference in the coordination energy between **1-SR** and **1-SeR** is 22.5 kcal/mol for R = Me and 27.1 kcal/mol for R = Ph, while the difference in ligand formation energy is 6.1 kcal/mol for R = Ph and 16.0 kcal/mol for R = Me, as shown by the value in the square bracket in Table 1.

The Au−Au interaction energy between the ligands is almost the same between the selenolate and thiolate analogues; see the potential energy curve against the distance of two neutral cyclic-$[Au(EMe)]_4$ in Figure 4. Hence, the ligand−ligand interaction is not the reason for the small formation energy of the thiolate nanocluster compounds. It is likely that one important reason for the smaller coordination energy of the thiolate analogues is the lower HOMO energies of the thiolate staple-like chain ligands $[Au_3(SR)_4]^-$ and $[Au_5(SR)_6]^-$ than those of the selenolate analogues, as shown in Table 2. As a result, the charge transfer (CT) from the staple-like chain ligand to the vacant orbital of the Au_8 core more strongly occurs in the selenolate species than in the thiolate ones, which contributes to the larger coordination energy of **1-SeR** than that of **1-SR**. It should be concluded that because the coordination of the selenolate ligands with the Au_8 core yields a much larger stabilization energy than that of the thiolate ones, the selenolate analogue **1-SeR** is more stable than the thiolate analogue.

The same discussion is possible in **2-SPh** and **2-SePh**. The formation energy of the thiolate staple-like chain ligand is moderately larger than that of the selenolate one but the difference is not very large (6.1 kcal/mol). On the other hand, the coordination of the selenolate staple-like chain ligand with the Au_8 core yields somewhat larger stabilization energy than that of the thiolate one by 12.6 kcal/mol; see Table 1. Hence, the formation of **2-SePh** is more favorable than that of **2-SPh**. When R = Me, however, the trend becomes different; the formation of **2-SMe** is more favorable than that of **2-SeMe**. This is because the formation energy of the thiolate staple-like chain ligand is larger than that of the selenolate one by about 16.0 kcal/mol, but the coordination energy of the selenolate staple-like chain ligand with the Au_8 core is moderately larger than that of the thiolate one by 11.2 kcal/mol; see Table 1. This result suggests that the use of alkyl group yields larger formation energy of the thiolate staple-like chain ligand, which compensates well the smaller coordination energy of the thiolate staple-like chain ligand with the Au_8 core. Thereby, the formation of **2-SMe** is more favorable than that of **2-SeMe**.

Here, we wish to mention the HOMO−LUMO energy gap of these cluster compounds. When the formation energy of a molecule is large, the HOMO−LUMO energy gap of the molecule is also large in general. However, it is not easy to discuss the stabilities of these cluster compounds based on the HOMO−LUMO energy gap because some other factor such as aurophilic interaction between entangled ligands participates in the stability; see Supporting Information Figure S6, Table S4, and Scheme S1, and discussion there.

It is noted that the formation energy of **2-SeR** is sufficiently large and is not different very much from that of **2-SR**. This result suggests that the synthesis of **2-SeR** is not difficult. Because the formation of **1-SeR** needs enough Au(SeR), it is likely that **2-SeR** can be synthesized as a stable species only when Au(SeR) is not present enough; if not, $[Au_5(SeR)_6]^-$ is sufficiently formed and thereby not **2-SeR** but **1-SeR** is synthesized.

It is concluded that the selenolate Au nanoclusters are more stable than the thiolate analogues because of the larger coordination energy between the Au_8 core and the staple-like chain ligand. It is expected that **2-SeR** would be formed if the concentration of Au(SeR) is carefully adjusted.

CONCLUSIONS

The selenolate-protected Au nanocluster **1-SePh** is theoretically investigated to elucidate the electronic structure of the unusual Au_8 core, clarify the reason why the staple-like chain ligand has an entangled geometry, and make comparison with **2-SePh** and the thiolate analogues. No suitable DFT functional is found for geometry optimization, especially for reproducing the Au^{3A}−Au^{3B}, Au^{3A}−Au^{4B}, Au^{4A}−Au^{3B}, and Au^{4A}−Au^{4B} distances. On the other hand, the SCS-MP2 method reproduces well these distances, suggesting that the aurophilic interaction plays an important role in determining the geometry and stability of the unusual $[Au_8]^{4+}$ core. Because the DFT method with the B3PW91 reproduces well the other geometrical parameters, a combination of the SCS-MP2 and the DFT with the B3PW91 is a good choice to optimize the geometry of this kind of nanocluster compound. Analysis of the electronic structure of **1-SePh** shows that the Au_8 core consists of two tetrahedral $[Au_4]^{2+}$ species. This tetrahedral $[Au_4]^{2+}$ moiety has a stable closed-shell singlet ground state. The tetrahedral structure of $[Au_4]^{2+}$ is more stable than the square-planar one, because of the large bonding overlap of the doubly occupied MO. These two tetrahedral $[Au_4]^{2+}$ species are surrounded and protected by the staple-like chain ligands. The coordination energy of the Au_8 core with the staple-like chain ligands is very large. The selenolate-protected Au nanocluster is more stable than the thiolate analogue because the coordination energy of the $[Au_8]^{4+}$ core with the selenolate staple-like chain ligand is larger than that with the thiolate ones. It is noted that the Au−Au attractive interaction (i.e., aurophilic interaction) exists between two staple-like chain ligands and between the Au_8 core and the staple-like chain ligand. This interaction plays an important role to realize the entangled geometries of **1-ER** and **2-ER** and also to stabilize the Au_{24} system **1-ER** more than the Au_{20} system **2-ER**; remember that more Au−Au interactions are involved in **1-ER** than in **2-ER**. Because the formation energy of **2-SeR** is large, the isolation of this compound would be possible when the concentration of Au(SeR) is carefully adjusted; if Au(SeR) is added in excess, **1-SeR** is easily formed because of the larger formation energy than that of **2-SeR**.

DOI: 10.1021/jacs.5b04337
J. Am. Chem. Soc. 2015, 137, 8593−8602

■ ASSOCIATED CONTENT

Supporting Information

The optimized geometrical parameters and discussion for **1-SePh** at the PBE, M06L, B3LYP, B3PW91, TPSSh, M06, B3LYP-D and B3LYP-D3 methods; effect of two f polarization functions, orbital energy diagram of square planar (D_{4h}) and tetrahedral (T_d) structures of $[Au_4]^{2+}$; NBO charges of $[Au_4]$ unit in **1-SePh**, **2-SePh**, **1-SPh**, **2-SPh**, **1-SeMe**, **2-SeMe**, **1-SMe**, and **2-SMe**; the HOMO shape of the staple-like chain ligands $[Au_3(SePh)_4]^-$ and $[Au_5(SePh)_6]^-$; potential energy curves of two cyclic-$[Au(SMe)]_4$ and two cyclic-$[Au(SeMe)]_4$ against the Au−Au distance; optimized structures of **1-SMe** and **2-SMe**; frontier orbital shape and energy of **1-SeMe**, **2-SeMe**, **1-SMe**, and **2-SMe** and discussion for them; comparison between selenolate and thiolate cluster compounds; complete ref 29; and the Cartesian coordinate and total energy of all the optimized structures in this work. The Supporting Information is available free of charge on the ACS Publications website at DOI: 10.1021/jacs.5b04337.

■ AUTHOR INFORMATION

Corresponding Author

*sakaki.shigeyoshi.47@st.kyoto-u.ac.jp

Notes

The authors declare no competing financial interest.

■ ACKNOWLEDGMENTS

The present work was supported by MEXT program "Elements Strategy Initiative to Form Core Research Center" (since 2012), MEXT; Ministry of Education Culture, Sports, Science and Technology, Japan. We wish to thank the computer center of Institute for Molecular Science (IMS, Okazaki, Japan) for kind use of computers and the RIKEN Advanced Institute for Computational Science (RIKEN AICS, Kobe, Japan; No. hp140109) for kind use of the K-computer. S.S. wishes to acknowledge the supports from the Ministry of Education, Culture, Science, Sport and Technology through Grants-in-Aid of Specially Promoted Science and Technology (No. 22000009), Grants-in-Aid for Scientific Research (No. 15H03770), and Japan Science and Technology Cooperation (CREST 'Establishment of Molecular Technology towards the Creation of New Functions' Area).

■ REFERENCES

(1) (a) Qian, H.; Zhu, M.; Wu, Z.; Jin, R. *Acc. Chem. Res.* **2012**, *45*, 1470. (b) Chaki, N. K.; Negishi, Y.; Tsunoyama, H.; Shichibu, Y.; Tsukuda, T. *J. Am. Chem. Soc.* **2008**, *130*, 8608.

(2) (a) Chen, J.; Zhang, Q.-F.; Bonaccorso, T. A.; Williard, P. G.; Wang, L.-S. *J. Am. Chem. Soc.* **2013**, *136*, 92. (b) Wan, X.-K.; Lin, Z.-W.; Wang, Q.-M. *J. Am. Chem. Soc.* **2012**, *134*, 14750. (c) Kamei, Y.; Shichibu, Y.; Konishi, K. *Angew. Chem., Int. Ed.* **2011**, *50*, 7442.

(3) (a) Maity, P.; Takano, S.; Yamazoe, S.; Wakabayashi, T.; Tsukuda, T. *J. Am. Chem. Soc.* **2013**, *135*, 9450. (b) Kobayashi, N.; Kamei, Y.; Shichibu, Y.; Konishi, K. *J. Am. Chem. Soc.* **2013**, *135*, 16078. (c) Maity, P.; Wakabayashi, T.; Ichikuni, N.; Tsunoyama, H.; Xie, S.; Yamauchi, M.; Tsukuda, T. *Chem. Commun.* **2012**, *48*, 6085. (d) Maity, P.; Tsunoyama, H.; Yamauchi, M.; Xie, S.; Tsukuda, T. *J. Am. Chem. Soc.* **2011**, *133*, 20123.

(4) (a) Meng, X.; Xu, Q.; Wang, S.; Zhu, M. *Nanoscale* **2012**, *4*, 4161. (b) Kurashige, W.; Yamaguchi, M.; Nobusada, K.; Negishi, Y. *J. Phys. Chem. Lett.* **2012**, *3*, 2649. (c) Xu, Q.; Wang, S.; Liu, Z.; Xu, G.; Meng, X.; Zhu, M. *Nanoscale* **2013**, *5*, 1176. (d) Kurashige, W.; Yamazoe, S.; Kanehira, K.; Tsukuda, K.; Negishi, Y. *J. Phys. Chem. Lett.* **2013**, *4*, 3181.

(5) (a) Li, G.; Zeng, C.; Jin, R. *J. Am. Chem. Soc.* **2014**, *136*, 3673.

(6) (a) Zhang, X.-D.; Luo, Z.; Chen, J.; Shen, X.; Song, S.; Sun, Y.; Fan, S.; Fan, F.; Leong, D. T.; Xie, J. *Adv. Mater.* **2014**, *26*, 4565. (b) Chen, Y.-S.; Choi, H.; Kamat, P. V. *J. Am. Chem. Soc.* **2013**, *135*, 8822. (c) Wu, Z.; Wang, M.; Yang, J.; Zheng, X.; Cai, W.; Meng, G.; Qian, H.; Wang, H.; Jin, R. *Small* **2012**, *8*, 2028.

(7) (a) Zhu, M.; Qian, H.; Jin, R. *J. Am. Chem. Soc.* **2009**, *131*, 7220. (b) Pei, Y.; Gao, Y.; Shao, N.; Zeng, X. C. *J. Am. Chem. Soc.* **2009**, *131*, 13619.

(8) (a) Zhu, M.; Qian, H.; Jin, R. *J. Phys. Chem. Lett.* **2010**, *1*, 1003. (b) Pei, Y.; Pal, R.; Liu, C.; Gao, Y.; Zhang, Z.; Zeng, X. C. *J. Am. Chem. Soc.* **2012**, *134*, 3015.

(9) A cationic species which includes similar Au_8 core has been reported after the report of $Au_{20}(SR)_{16}$ (R = CH_2CH_2Ph), $Au_{24}(SR)_{20}$ (R = CH_2CH_2Ph), and $Au_{24}(SeR)_{20}$ (R = Ph). Kobayashi, N.; Kamei, Y.; Shichibu, Y.; Konishi, K. *J. Am. Chem. Soc.* **2013**, *135*, 16078.

(10) Häkkinen, H.; Walter, M.; Grönbeck, H. *J. Phys. Chem. B* **2006**, *110*, 9927.

(11) (a) Crasto, D.; Barcaro, G.; Stener, M.; Sementa, L.; Fortunelli, A.; Dass, A. *J. Am. Chem. Soc.* **2014**, *136*, 14933. (b) Zeng, C.; Liu, C.; Chen, Y.; Rosi, N. L.; Jin, R. *J. Am. Chem. Soc.* **2014**, *136*, 11922. (c) Jiang, D.; Whetten, R. L.; Luo, W.; Dai, S. *J. Phys. Chem. C* **2009**, *113*, 17291. (d) Heaven, M. W.; Dass, A.; White, P. S.; Holt, K. M.; Murray, R. W. *J. Am. Chem. Soc.* **2008**, *130*, 3754. (e) Zhu, M.; Aikens, C. M.; Hollander, F. J.; Schatz, G. C.; Jin, R. *J. Am. Chem. Soc.* **2008**, *130*, 5883. (f) Jadzinsky, P. D.; Calero, G.; Ackerson, C. J.; Bushnell, D. A.; Kornberg, R. D. *Science* **2007**, *318*, 430. (g) Wiseman, M. R.; Marsh, P. A.; Bishop, P. T.; Brisdon, B. J.; Mahon, M. F. *J. Am. Chem. Soc.* **2000**, *122*, 12598.

(12) Song, Y.; Wang, S.; Zhang, J.; Kang, X.; Chen, S.; Li, P.; Sheng, H.; Zhu, M. *J. Am. Chem. Soc.* **2014**, *136*, 2963.

(13) Grimme, S. J. *Chem. Phys.* **2003**, *118*, 9095.

(14) (a) Becke, A. D. *Phys. Rev.* **1988**, *A38*, 3098. (b) Becke, A. D. *J. Chem. Phys.* **1993**, *98*, 5648.

(15) Perdew, J. P.; Wang, Y. *Phys. Rev.* **1992**, *B45*, 13244.

(16) (a) Perdew, J. P.; Burke, K.; Ernzerhof, M. *Phys. Rev. Lett.* **1996**, *77*, 3865. (b) Perdew, J. P.; Burke, K.; Ernzerhof, M. *Phys. Rev. Lett.* **1997**, *78*, 1396.

(17) Zhao, Y.; Truhlar, D. G. *J. Chem. Phys.* **2006**, *125*, 194101.

(18) Lee, C.; Yang, W.; Parr, R. G. *Phys. Rev.* **1988**, *B37*, 785.

(19) Tao, J. M.; Perdew, J. P.; Staroverov, V. N.; Scuseria, G. E. *Phys. Rev. Lett.* **2003**, *91*, 146401.

(20) Zhao, Y.; Truhlar, D. G. *Theor. Chem. Acc.* **2008**, *120*, 215.

(21) Grimme, S. *J. Comput. Chem.* **2006**, *27*, 1787.

(22) Grimme, S.; Antony, J.; Ehrlich, S.; Krieg, H. *J. Chem. Phys.* **2010**, *132*, 154104.

(23) (a) Hay, P.; Wadt, W. R. *J. Chem. Phys.* **1985**, *82*, 299−310. (b) Wadt, W. R.; Hay, P. J. *J. Chem. Phys.* **1985**, *82*, 299.

(24) Höllwarth, A.; Böhme, M.; Dapprich, S.; Ehlers, A. W.; Gobbi, A.; Jonas, V.; Köhler, K. F.; Stegmann, R.; Veldkamp, A.; Frenking, G. *Chem. Phys. Lett.* **1993**, *208*, 237.

(25) (a) Hehre, W. J.; Ditchfield, R.; Pople, J. A. *J. Chem. Phys.* **1972**, *56*, 2257. (b) Hariharan, P. C.; Pople, J. A. *Theor. Chim. Acta* **1973**, *28*, 213. (c) Francl, M. M.; Petro, W. J.; Hehre, W. J.; Binkley, J. S.; Gordon, M. S.; DeFrees, D. J.; Pople, J. A. *J. Chem. Phys.* **1982**, *77*, 3654.

(26) (a) Andrae, D.; Haeussermann, U.; Dolg, M.; Stoll, H.; Preuss, H. J. *Theor. Chim. Acta* **1990**, *77*, 123. (b) Bergner, A.; Dolg, M.; Kuechle, W.; Stoll, H.; Preuss, H. *Mol. Phys.* **1993**, *80*, 1431.

(27) We examined the effects of two f polarization functions on the potential energy surface against the Au−Au distance between two $[Au(EMe)]_4$ molecules. The addition of two f polarization functions[28] changes the optimized Au−Au distance little, but increases the binding energy by about 5 kcal/mol. However, the binding energy after correction of basis set superposition error is similar to that calculated without f function, suggesting that the binding energy calculated by the SCS-MP2/BS-2 without f polarization function is not very unreasonable in a practical sense; see Figure S4, Table S2, and discussion there in the Supporting Information for details.

(28) Martin, J. M. L.; Sundemann, A. *J. Chem. Phys.* **2001**, *114*, 3408.

DOI: 10.1021/jacs.5b04337
J. Am. Chem. Soc. 2015, 137, 8593−8602

(29) Frisch, M. J.; et al. *Gaussian 09*, revision D.01; Gaussian, Inc.: Wallingford, CT, 2013.
(30) NTChem 2013. http://labs.aics.riken.jp/nakajimat_top/ntchem_e.html, Nakajima, T.; Katouda, M.; Kamiya, M.; Nakatsuka, Y. *Int. J. Quantum Chem.* **2015**, *115*, 349.
(31) Ishimura, K. SMASH-1.1.0. http://smash-qc.sourceforge.net/.
(32) Pyykkö, P.; Xiong, X. G.; Li, J. *Faraday Discuss.* **2011**, *152*, 169.
(33) Because the Au_8 core has a symmetrical structure, X^1 and X^2 are defined at the midpoints of the Au^{3A}–Au^{4A} and Au^{3B}–Au^{4B} bonds; see the inset of Figure 1. All geometrical parameters except for the X^1–X^2 distance were optimized with the B3PW91 at several fixed X^1–X^2 distances. Thus-obtained geometry was employed in the MP2 and SCS-MP2 calculations.
(34) (a) Pyykkö, P.; Runeberg, N. *J. Chem. Soc., Chem. Commun.* **1993**, 1812. (b) Zeller, E.; Beruda, H.; Schmidbaur, H. *Inorg. Chem.* **1993**, *32*, 3203.
(35) The φ_1^{Au8} becomes the most stable around $\theta = 55°$ but then moderately less stable in **Conf-II**. Around $\theta = 55°$, a moderate bonding overlap is formed between two $[Au_4]^{2+}$ species; see Figure 3. However, its antibonding overlap is induced in the other φ_2^{Au8} and φ_3^{Au8}, which destabilizes these φ_2^{Au8} and φ_3^{Au8} MOs in energy around $\theta = 55°$. This is because these MOs are constructed by two doubly occupied MOs of the $[Au_4]^{2+}$ species. Also, the steric repulsion is favorable in **Conf-II**. Hence, not the structure of $\theta = 55°$ but **Conf-II** is the most stable.
(36) Because the NBO charge of the $[Au_4]^{2+}$ moiety is not +2.0 but much smaller in these Au cluster compounds, the electrostatic interaction between two $[Au_4]$ moieties is not very repulsive in these nanocluster compounds; see Table S3 in the Supporting Information for the NBO charge of the $[Au_4]$ moiety.
(37) Cyclic-$[Au(SePh)]_4$ was taken as a starting compound because this was reported as the most stable adduct of four Au(SeR) molecules; Bonasia, P.; Gindelberger, D. E.; Arnold. *J. Inorg. Chem.* **1993**, *32*, 5126.
(38) Because cyclic-$[Au(SePh)]_4$ corresponds to $11/2[Au(SePh)]_4$, the stoichiometry is kept here.
(39) Because the staple-like chain ligand is negatively charged, the aurophilic interaction cannot be correctly evaluated with such ligand due to the presence of electrostatic repulsion. This is the reason why we employed a cyclic-$[Au(SeMe)]_4$ molecule to evaluate the Au–Au interaction.
(40) (a) Sakaki, S.; Biswas, B.; Sugimoto, M. *Organometallics* **1998**, *17*, 1278. (b) Sakaki, S.; Kai, S.; Sugimoto, M. *Organometallics* **1999**, *18*, 4825. (c) Sakaki, S.; Biswas, B.; Musashi, Y.; Sugimoto, M. *J. Organomet. Chem.* **2000**, *611*, 288. (d) Ray, M.; Nakao, Y.; Sato, H.; Sakaki, S. *Organometallics* **2007**, *26*, 4413. (e) Sugiyama, A.; Ohnishi, Y.-y.; Nakaoka, M.; Nakao, Y.; Sato, H.; Sakaki, S.; Nakao, Y.; Hiyama, T. *J. Am. Chem. Soc.* **2008**, *130*, 12975.

DOI: 10.1021/jacs.5b04337
J. Am. Chem. Soc. 2015, 137, 8593–8602